

Repeated drainage from megathrusts during episodic slow slip

Junichi Nakajima^{1*} and Naoki Uchida²

Pore-fluid pressure levels are considered to regulate the frictional strength and slip behaviour at megathrusts, where the largest earthquakes on Earth occur. Some analyses have suggested that the breaking of permeability seals during megathrust earthquakes causes subsequent drainage from the megathrust. However, it is poorly understood whether drainage follows frequent occurrences of episodic slow slip events. Here we analyse seismic waveform data beneath Kanto, Japan, for the period from 2004 to 2015 and show that seismicity rates and seismic attenuation above the megathrust of the Philippine Sea slab change cyclically in response to accelerated slow slip. These observations are interpreted to represent intensive drainage during slow slip events that repeat at intervals of approximately one year and subsequent migration of fluids into the permeable overlying plate. Our observations suggest that if slow slip events occur under an impermeable overlying plate, fluids draining due to slow slip events could be forced to channel within the megathrust, potentially enhancing pore-fluid pressure at an up-dip, locked seismogenic megathrust. This process might increase the potential to trigger large earthquakes near slow slip areas. Although stress transfer is recognized as an important factor for triggering megathrust failure, fluid transfer accompanied by episodic slow slip events will thus play an additional and crucial part in megathrust weakening.

Conventional wisdom has held that subduction megathrusts slip either as earthquakes or through stable creep¹. However, recent observations have shown that in many subduction zones slow slip events (SSEs) recur at intervals ranging from months to years^{2–4}. Aseismic SSEs are considered to be part of the wide spectrum of slip behaviour that exists at megathrusts⁵, and stress transfer due to SSEs is an important factor contributing to an increase in the potential for megathrust earthquake occurrence⁶. Substantial short-term stress loading due to SSEs may have triggered the dynamic rupture of the moment magnitude $M_w = 9.0$ 2011 Tohoku-oki earthquake⁷, and a recent observation in northeast Japan found concentrated occurrences of the JMA (Japan Meteorological Agency) magnitude $M_{\text{JMA}} \geq 5$ earthquakes during SSE periods repeating at intervals of 1–6 years⁸. These observations suggest that stress perturbations due to SSEs have an essential role in modulating earthquake occurrence time.

Observations following large megathrust earthquakes have suggested that drainage occurs from megathrusts, based on increases in V_p/V_s ratio (P-wave to S-wave velocity ratio)⁹ and seismic activity¹⁰ above the megathrust, seismicity migrating into the overlying plate¹¹, stress regime changes in the overlying plate¹² and a sharp increase in mantle-derived helium concentrations in bottom seawater¹³. Although no studies have shown drainage following episodic SSEs, SSEs can potentially drain fluids from megathrusts because slow slip areas retain extremely high, near-lithostatic pore-fluid pressures^{5,14,15}. SSEs repeat at short intervals ranging from months to years, often occurring at the down-dip end of a locked portion of the seismogenic megathrust⁶. Therefore, revealing whether drainage occurs in response to episodic SSEs is important for quantifying temporal changes in the frictional strength at the megathrust in regions neighbouring SSEs.

Correlation of supraslab seismicity with SSEs

In this paper, we investigate a pair of seismic clusters beneath Kanto, Japan (indicated by the dashed rectangle in Fig. 1a). The deep

earthquake cluster is a seismic streak on the Philippine Sea slab megathrust at depths of 40–60 km, whereas the shallower supraslab cluster is concentrated at depths of 25–35 km. The megathrust earthquake cluster includes small repeating earthquakes¹⁶. We applied the double-difference technique¹⁷ to differential arrival-time data for 2,965 megathrust earthquakes and 225 supraslab earthquakes ($M \geq 1$) reported in the unified JMA hypocentre catalogue from January 2004 to December 2015 and relocated the earthquakes with the JMA2001 model¹⁸. Relocated megathrust earthquakes are distributed along a dipping plane that is consistent with the slab surface dip¹⁹, whereas supraslab earthquakes are located above the up-dip end of the megathrust earthquakes with a gap of about 5 km (Fig. 1c). Earthquakes in the supraslab seismic cluster have normal-fault and strike-slip mechanisms, with an east–west-oriented tensional (T) axis. Supraslab earthquakes increased following the 2011 Tohoku-oki earthquake (Fig. 2a); however, their focal mechanisms did not change substantially after the Tohoku-oki earthquake (Fig. 1b, inset and Supplementary Fig. 1).

We investigated temporal correlations between supraslab seismicity and megathrust slip. First, we counted the number of supraslab earthquakes in a 0.4-year time window with a 0.1-year moving window (Fig. 2a). Then we considered small repeating earthquakes (red stars in Fig. 1c) that occurred within a $\pm 3\sigma$ (standard deviation) distance from the epicentral centroid of the supraslab seismic cluster, and estimated the average slip rates on the megathrust from repeater sequences following Uchida et al.⁸ using the same time-window length as in the supraslab cluster analysis (see Method for slip rate estimates). Estimated slip rates, which can be used as proxies for slow slip on the megathrust⁸, appeared to accelerate periodically (Fig. 2b), suggesting the occurrences of SSEs at approximately 1-year intervals.

We carried out cross-correlation analysis to evaluate temporal correlations between the time series of the number of supraslab earthquakes and megathrust slip rates for periods from 2004 to 2010

¹Department of Earth and Planetary Sciences, School of Science, Tokyo Institute of Technology, Tokyo, Japan. ²Research Center for Prediction of Earthquakes and Volcanic Eruptions, Graduate School of Science, Tohoku University, Sendai, Japan. *e-mail: nakajima@geo.titech.ac.jp

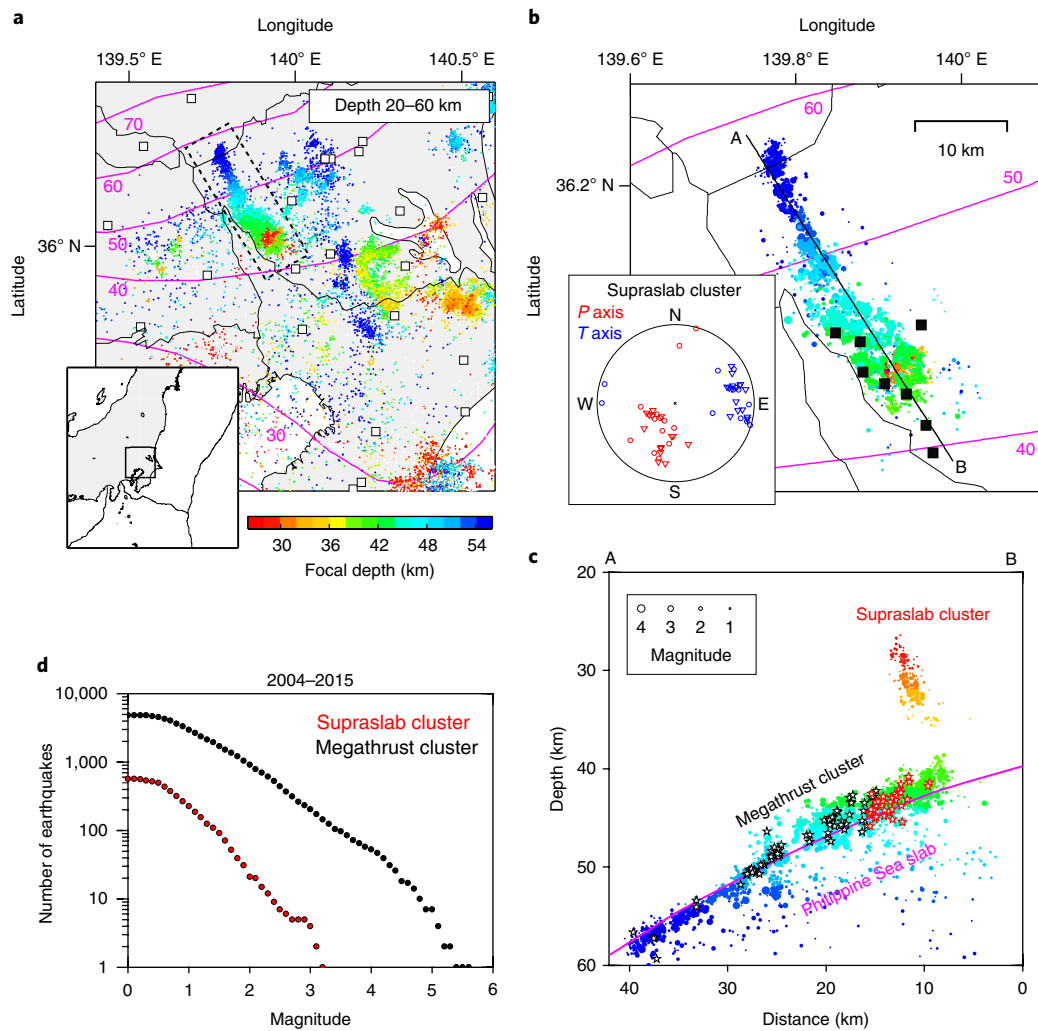


Fig. 1 | Analysed seismicity. a, Map showing seismicity (coloured circles) from 2004 to 2015, permanent seismograph stations (white squares) and the upper surface of the Philippine Sea slab¹⁹ (pink lines) in the rectangle area in the inset map. **b**, Relocated earthquakes (coloured circles) in the dashed rectangle in **a**. Black squares denote the eight Metropolitan Seismic Observation Network stations. The inset shows the lower-hemisphere distribution of the *P* and *T* axes of the focal mechanisms for 26 supraslab earthquakes. Circles and triangles denote the *P* and *T* axes for earthquakes occurring before and after the 2011 Tohoku-oki earthquake²⁰. **c**, Cross-section along A–B in **b**. Stars represent repeating earthquakes¹⁶, and red stars are repeaters used to estimate megathrust slip rates. **d**, Frequency–magnitude (M_{JMA}) distributions of supraslab and megathrust earthquakes.

and 2013 to June 2015 (2015.5) (see Methods for correlation analysis). We did not use data from 2011 and 2012 because the number of supraslab earthquakes greatly increased (Fig. 2a), as a result of the static stress change and postseismic deformation caused by the 2011 Tohoku-oki earthquake²⁰. Calculated cross-correlation coefficients indicating a moderate positive correlation suggest that supraslab seismicity followed accelerated megathrust slip at 0.2–0.4-year lags for 2004–2010 and a 0.1-year lag for 2013–2015.5, within a <1% significance level (Fig. 2c). We obtained the same lag times using different window lengths (Supplementary Fig. 2a and 2b), thus demonstrating the robustness of the lag times observed between the two processes.

Seismic attenuation changes in response to slow slip

To investigate temporal changes in seismic properties above the megathrust during the inferred SSEs, we analysed waveform data recorded at eight Metropolitan Seismic Observation Network (MeSO-net) stations²¹ (black squares in Fig. 1b) from July 2009 to June 2015. We estimated P-wave attenuation (Q_p^{-1}) between the two seismic clusters using the decay rate of the P-wave spectral ratio for

a pair of earthquakes, one from the megathrust cluster and one from the supraslab cluster (Method and Supplementary Figs. 3 and 4). We used earthquakes in the megathrust cluster that occurred in each 0.4-year window length and shifted the window by 0.1 year to resolve the time-dependent Q_p^{-1} above the megathrust. We analysed the same set of supraslab earthquakes for all time periods to avoid the influence of different sets of supraslab earthquakes on the Q_p^{-1} estimate.

The obtained Q_p^{-1} values show temporal fluctuations beyond estimation errors (Fig. 3a), and the Q_p^{-1} temporal variation can be constrained by changes in the slope of spectral ratios (Fig. 3b and Supplementary Fig. 5). Calculated cross-correlation coefficients for 2013–2015.5 indicate, within a <1% significance level (P -value < 0.01), that the observed Q_p^{-1} and megathrust slip rates are strongly positively correlated at very short lags of 0–0.1 years (cross-correlation coefficients of about 0.8) or negatively correlated at a positive lag of 0.5 year and negative lags of 0.4–0.5 years (Fig. 3c). Given that the number of supraslab earthquakes correlates with megathrust slip rates at a short positive lag of 0.1 year (right panel in Fig. 2c), we consider that the highest cross-correlation coefficients at lags of 0–0.1 years reflect a physical process that

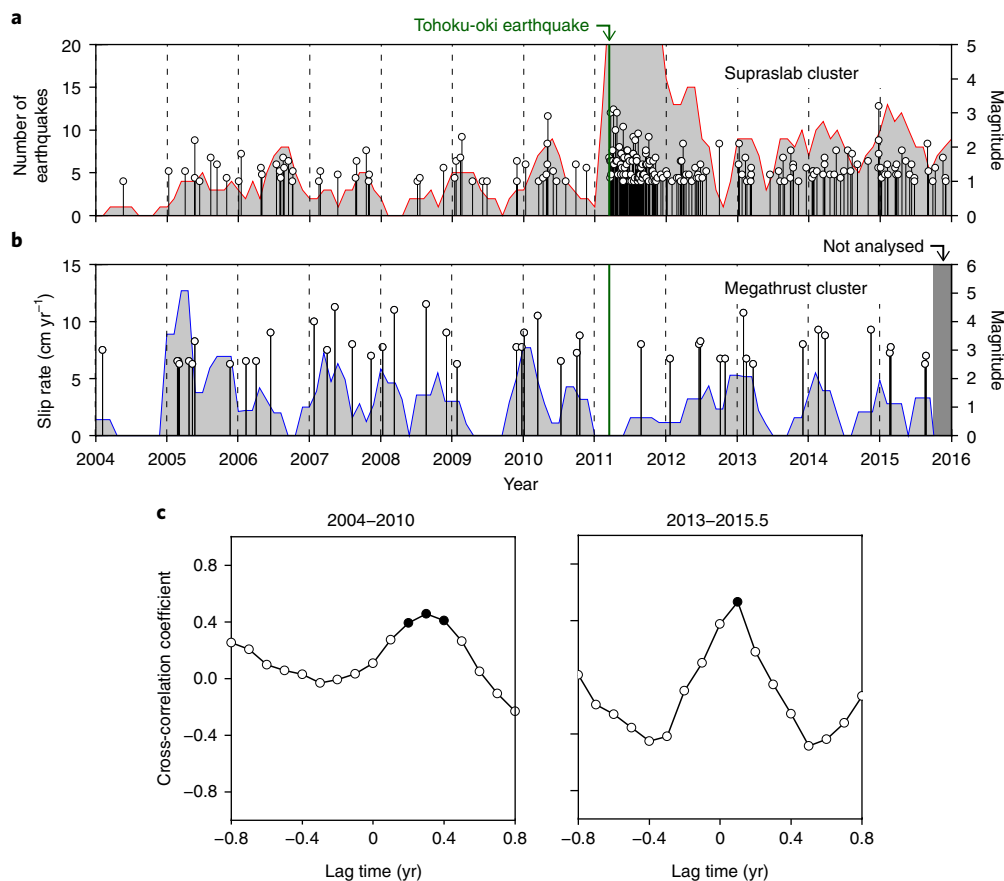


Fig. 2 | Correlation between supraslab earthquakes and megathrust slip rates. **a**, The number of supraslab earthquakes counted for 0.4-year time windows with a 0.1-year moving window (grey histogram) and a magnitude (M_{MA})–time plot (white circles). **b**, Average slip rates on the megathrust (grey histogram) estimated from the repeating earthquakes shown by red stars in Fig. 1c. **c**, Cross-correlation coefficient between supraslab seismicity and megathrust slip rates for 2004–2010 (left) and 2013–2015.5 (right). Solid symbols indicate cross-correlation coefficients at which the null hypothesis that supraslab earthquakes occur randomly irrespective of megathrust slip is rejected with a probability of $<1\%$ ($P < 0.01$). Positive lag means that supraslab seismicity is delayed with respect to the megathrust slip.

occurs in response to SSEs and attenuation is enhanced concurrently with SSEs. The relatively high negative correlations at lags of ± 0.4 – 0.5 years may be due to a half-cycle skipping of semi-annual variations in Q_p^{-1} and megathrust slip rates.

Cyclic drainage from the megathrust

A possible mechanism for explaining the observed temporal correlations among SSEs, supraslab seismicity, and Q_p^{-1} changes is stress transfer by each SSE, potentially triggering seismicity²⁰ and enhancing Q_p^{-1} through increased dislocation density²². However, stress change alone cannot satisfactorily account for the 0.2–0.4-year lags for 2004–2010 and the 0.1-year lag for 2013–2015.5 observed between supraslab seismicity and SSEs. Moreover, dislocation damping, which is a thermally activated process²², may not effectively work immediately above the megathrust, where repeating earthquakes occur and temperatures are probably below 350°C ²³. Even if increases in dislocation density due to stress transfer could enhance attenuation, an opposite sense of stress changes would be required for reducing attenuation during inter-slip periods. Therefore, we consider stress transfer not to be the sole cause of supraslab seismicity and attenuation enhancement in response to SSEs, although it may partially contribute.

We propose that the observed temporal correlations are attributed to the repeated evolution of flux at the megathrust. A low-permeability seal in the overpressurized megathrust breaks during SSEs, as observed for megathrust earthquakes^{9–13} (Fig. 4a). When fluids

draining from the megathrust saturate the rock above, seismic wave propagation enhances grain-scale dispersion (squirt flow)^{24,25} and attenuation increases without a significant delay (almost zero lag) from the inferred drainage. Subsequent fluid migration into the overlying plate triggers supraslab seismicity in spots where the permeability is low enough for pore-fluid pressure to increase efficiently to near-lithostatic values. The lags of 0.1–0.4 years for triggering earthquakes probably reflect the amount of time required for fluids to percolate approximately 5 km upward and for the pore-fluid pressure to increase to bring the system into brittle failure. The megathrust is then resealed by cementation in the active hydrothermal environment¹², and the pore-fluid pressure at the megathrust gradually increases over time owing to recharging of dehydrated fluids from the underlying hydrated crust²⁶. Because fluids are not supplied to the overlying plate during inter-slip periods, supraslab seismicity becomes quiescent and Q_p^{-1} is therefore reduced (Fig. 4b). The megathrust slips again when pore-fluid pressure increases and frictional strength falls below the shear stress acting on the megathrust. A wide range of SSE recurrence intervals observed worldwide may be governed by megathrust local flux balance instead of by the regional tectonic loading rate²⁷.

Permeability estimate

This study suggests that fluids draining from the megathrust during SSEs permeate into the overlying plate, thereby triggering supraslab earthquakes and enhancing seismic attenuation. Fluid transport into the overlying plate may result either from

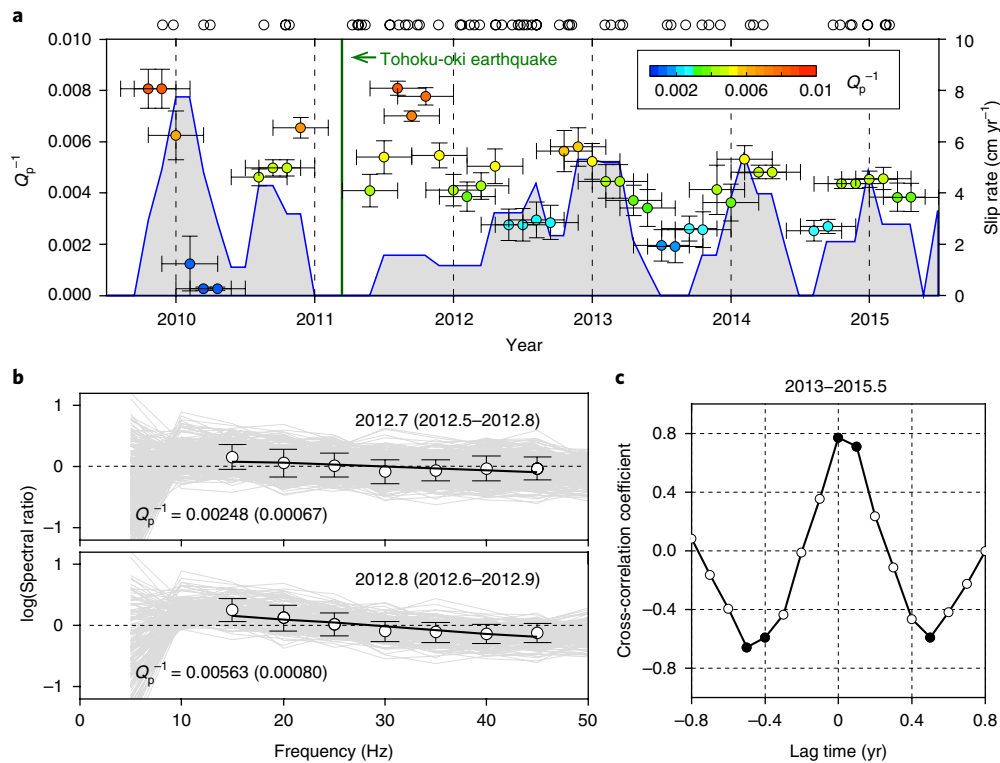


Fig. 3 | Temporal variation in P-wave attenuation, Q_p^{-1} . **a**, Values of Q_p^{-1} (coloured circles) with one standard deviation (vertical bars). Horizontal bars denote the time window length of each with taking care of the term, Q_p^{-1} estimate. The grey histogram shows megathrust slip rates (Fig. 2b). The circles above the panel denote the date of analysed megathrust earthquakes. **b**, Examples of spectral ratios of earthquakes for two periods. Grey lines represent each observation, and circles are the averaged spectral ratios at 5 Hz intervals with one standard deviation (vertical bars). The black line denotes the least-squares fitting, and the obtained Q_p^{-1} is shown with estimation error in parentheses. **c**, Cross-correlation coefficient between Q_p^{-1} and megathrust slip rates for 2013–2015.5. Solid symbols indicate cross-correlation coefficients with a probability value of <0.01 . Positive lag means that the change in Q_p^{-1} is delayed with respect to the megathrust slip.

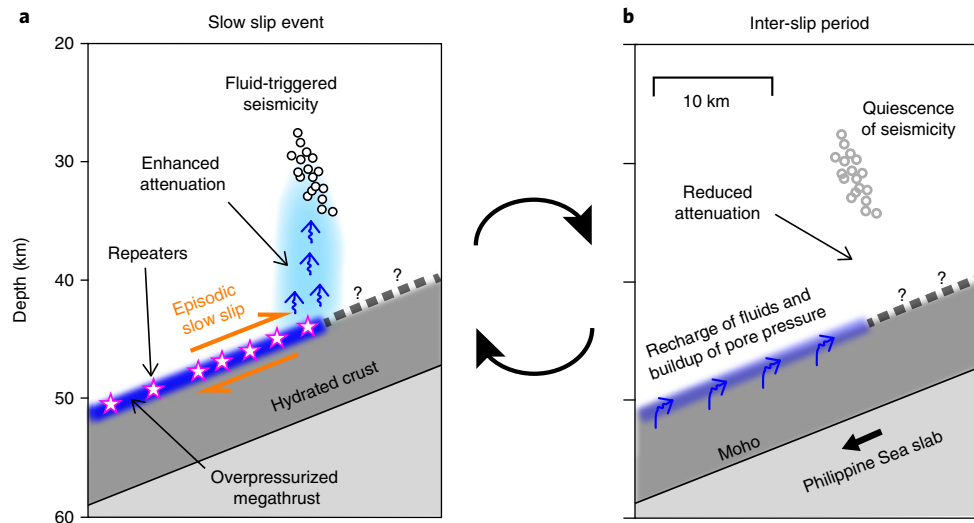


Fig. 4 | Schematic interpretation of drainage process. **a**, Slow slip event. **b**, Inter-slip period. The hydrated crust is constrained by tomographic imaging¹⁹.

the inherent permeable nature of the overlying plate or from a transient increase in the permeability due to SSEs. Recent studies have shown that the overlying plate is less metamorphosed above areas of episodic tremor and slip²⁸, and that the number of supraslab earthquakes is inversely correlated with regional episodic tremor and slip activity^{28,29}, suggesting that the permeation of fluids into the overlying plate is limited above areas

of episodic tremor and slip. Therefore, it is unlikely that the permeability above the megathrust is enhanced during SSEs to high enough values to enable large amounts of fluids to percolate transiently into the overlying plate. The supraslab seismic cluster analysed in this study may be facilitated by the presence of an inherent permeable zone at the up-dip end of the inferred slow slip area.

We estimate the permeability of an inferred permeable zone between the megathrust and supraslab seismic clusters using a relation from ref. ³⁰, $k = \beta \eta l^2 / \tau$. Permeability (k) is expressed as a function of the characteristic time (τ), length scale of the process (l), specific storage coefficient (β), and dynamic viscosity (η). Given l of 5 km, β of 10^{-10} Pa^{-1} for low-porosity rocks, and η of 10^{-4} Pa s as assumed in ref. ¹¹, we obtain the permeability of $2\text{--}4 \times 10^{-14} \text{ m}^2$ for τ of 0.2–0.4 years in 2004–2010 and $8 \times 10^{-14} \text{ m}^2$ for τ of 0.1 year in 2013–2015.5. The values we obtained fall in the upper limit of the permeability range ($10^{-13}\text{--}10^{-19} \text{ m}^2$) inferred above a megathrust at depths of 40–60 km^{9–11,31}. Such high permeability values suggest the presence of a highly fractured, pre-existing mature pathway to the supraslab cluster. Tensional stress caused by the Tohoku-oki earthquake³² may have forced the permeability of the fluid pathway to increase, shortening lag times to the activation of supraslab seismicity after the Tohoku-oki earthquake.

Implications for possible fluid transfer by slow slip

Because episodic tremor and slip tend to occur beneath the impermeable overlying plate^{28,33}, where a significant increase in the permeability is unlikely to occur transiently during slow slip, fluids may be forced to channel within the megathrust during and after SSEs. We hypothesize that in undrained conditions, fluids liberated by SSEs infiltrate the up-dip, elevating pore-fluid pressure at a locked portion of a seismogenic megathrust, which may increase the potential for triggering megathrust earthquakes. SSEs may have two functions triggering megathrust earthquakes: stress transfer that leads to a loading-rate change, as has been conventionally considered^{6–8,34}, and fluid transfer that reduces the frictional strength of the megathrust by increasing pore-fluid pressure. It may be essential to consider fluid transfer to a locked portion during episodic SSEs, which has not been fully simulated in seismic-cycle numerical calculations, to improve forecasts of future megathrust earthquakes in neighbouring slow slip regions.

The combination of megathrust drainage and triggered seismicity that we observed in this study shows behaviours like those observed in fluid-injection experiments. Fluid-injection experiments have shown that the number of earthquakes correlates with quantity changes in fluid injection³⁵, that seismicity quiescence follows the injection volume and pressure minima³⁶, and that temporal changes in seismic properties occur during fluid injection³⁷. Our observations suggest that a physical process similar to what occurs in near-surface fluid-injection experiments is happening at depth in the natural environment. The approximately 5-km gap between the two seismic clusters suggests that the passage of fluids is not solely sufficient to trigger earthquakes. This indicates that seismicity is facilitated by pore-fluid pressure building to near-lithostatic values and seismicity ceases when pressure drops.

Methods

Methods, including statements of data availability and any associated accession codes and references, are available at <https://doi.org/10.1038/s41561-018-0090-z>.

Received: 16 August 2017; Accepted: 27 February 2018;

Published online: 09 April 2018

References

- Lay, T., Kanamori, H. & Ruff, L. J. The asperity model and the nature of large subduction zone earthquakes. *Earthq. Predict. Res.* **1**, 3–71 (1982).
- Obara, K., Hirose, H., Yamamizu, F. & Kasahara, K. Episodic slow slip events accompanied by non-volcanic tremors in southwest Japan subduction zone. *Geophys. Res. Lett.* **31**, L23602 (2004).
- Rogers, G. & Dragert, H. Episodic tremor and slip on the Cascadia subduction zone: the chatter of silent slip. *Science* **300**, 1942–1943 (2003).
- Wallace, L. M. & Eberhart-Phillips, D. Newly observed, deep slow slip events at the central Hikurangi margin, New Zealand: implications for downdip variability of slow slip and tremor, and relationship to seismic structure. *Geophys. Res. Lett.* **40**, 5393–5398 (2013).
- Peng, Z. & Gombert, J. An integrated perspective of the continuum between earthquakes and slow-slip phenomena. *Nat. Geosci.* **3**, 599–607 (2010).
- Obara, K. & Kato, A. Connecting slowearthquakes to huge earthquakes. *Science* **353**, 253–257 (2016).
- Kato, A. et al. Propagation of slow slip leading up to the 2011 M_w 9.0 Tohoku-Oki earthquake. *Science* **335**, 705–708 (2012).
- Uchida, N., Iinuma, T., Nadeau, R. M., Bürgmann, R. & Hino, R. Periodic slow slip triggers megathrust zone earthquakes in northeastern Japan. *Science* **351**, 488–492 (2016).
- Husen, S. & Kissling, E. Postseismic fluid flow after the large subduction earthquake of Antofagasta, Chile. *Geology* **29**, 847–850 (2002).
- Nakajima, J., Yoshida, K. & Hasegawa, A. An intraslab seismic sequence activated by the 2011 Tohoku-oki earthquake: evidence for fluid-related embrittlement. *J. Geophys. Res. Solid Earth* **118**, 3492–3505 (2013).
- Nippress, S. E. J. & Rietbrock, A. Seismogenic zone high permeability in the Central Andes inferred from relocations of micro-earthquakes. *Earth Planet. Sci. Lett.* **263**, 235–245 (2007).
- Sibson, R. H. Stress switching in subduction forearcs: implications for overpressure containment and strength cycling on megathrusts. *Tectonophysics* **600**, 142–152 (2013).
- Sano, Y. et al. Helium anomalies suggest a fluid pathway from mantle to trench during the 2011 Tohoku-Oki earthquake. *Nat. Commun.* **5**, 3084 (2014).
- Seno, T. Determination of the pore fluid pressure ratio at seismogenic megathrusts in subduction zones: implications for strength of asperities and Andean-type mountain building. *J. Geophys. Res.* **114**, B05405 (2009).
- Kitajima, H. & Saffer, D. M. Elevated pore pressure and anomalously low stress in regions of low frequency earthquakes along the Nankai Trough subduction megathrust. *Geophys. Res. Lett.* **39**, L23301 (2012).
- Uchida, N., Asano, Y. & Hasegawa, A. Acceleration of regional plate subduction beneath Kanto, Japan, after the 2011 Tohoku-oki earthquake. *Geophys. Res. Lett.* **43**, 9002–9008 (2016).
- Waldhauser, F. & Ellsworth, W. L. A double-difference earthquake location algorithm: method and application to the Northern Hayward Fault, California. *Bull. Seismol. Soc. Am.* **90**, 1353–1368 (2000).
- Ueno, H., Hatakeyama, S., Aketagawa, T., Funasaki, J. & Hamada, N. Improvement of hypocenter determination procedures in the Japan Meteorological Agency (in Japanese with English abstract). *Q. J. Seismol.* **65**, 123–134 (2002).
- Nakajima, J., Hirose, F. & Hasegawa, A. Seismotectonics beneath the Tokyo metropolitan area, Japan: effect of slab-slab contact and overlap on seismicity. *J. Geophys. Res.* **114**, B08309 (2009).
- Toda, S., Stein, R. S. & Lin, J. Widespread seismicity excitation throughout central Japan following the 2011 $M=9.0$ Tohoku earthquake and its interpretation by Coulomb stress transfer. *Geophys. Res. Lett.* **38**, L00G03 (2011).
- Sakai, S. & Hirata, N. Distribution of the Metropolitan Seismic Observation network (in Japanese with English abstract). *Bull. Earthq. Res. Inst. Tokyo Univ.* **84**, 57–69 (2009).
- Farla, R. J. M., Jackson, I., Fitz Gerald, J. D., Faul, U. H. & Zimmerman, M. E. Dislocation damping and anisotropic seismic wave attenuation in Earth's upper mantle. *Science* **336**, 332–335 (2012).
- Hyndman, R. D., Yamano, M. & Oleskevich, D. A. The seismogenic zone of subduction thrust faults. *Island Arc* **6**, 244–260 (1997).
- Gurevich, B., Makarynska, D., de Paula, O. B. & Pervukhina, M. A simple model for squirt-flow dispersion and attenuation in fluid-saturated granular rocks. *Geophysics* **75**, N109–N120 (2010).
- Müller, T. M., Gurevich, B. & Lebedev, M. Seismic wave attenuation and dispersion resulting from wave-induced flow in porous rocks—a review. *Geophysics* **75**, 75A147–75A164 (2010).
- Hyndman, R. D. & Peacock, S. M. Serpentinization of the forearc mantle. *Earth Planet. Sci. Lett.* **212**, 417–432 (2003).
- Chen, K. H., Nadeau, R. M. & Rau, R. J. Towards a universal rule on the recurrence interval scaling of repeating earthquakes? *Geophys. Res. Lett.* **34**, L16308 (2007).
- Nakajima, J. & Hasegawa, A. Tremor activity inhibited by well-drained conditions above a megathrust. *Nat. Commun.* **7**, 13863 (2016).
- Boyarko, D. C. & Brudzinski, M. R. Spatial and temporal patterns of nonvolcanic tremor along the southern Cascadia subduction zone. *J. Geophys. Res.* **115**, B00A22 (2010).
- Townend, J. & Zoback, M. D. How faulting keeps the crust strong. *Geology* **28**, 399–402 (2000).
- Koerner, A., Kissling, E. & Miller, S. A. A model of deep crustal fluid flow following the $M_w=8.0$ Antofagasta, Chile, earthquake. *J. Geophys. Res.* **109**, B06307 (2004).
- Yoshida, K. et al. Stress before and after the 2011 great Tohoku-oki earthquake and induced earthquakes in inland areas of eastern Japan. *Geophys. Res. Lett.* **39**, L03302 (2012).

33. Wells, R. E., Blakely, R. J., Wech, A. G., McCrory, P. A. & Michael, A. Cascadia subduction tremor muted by crustal faults. *Geology* **45**, 515–518 (2017).
34. Segall, P. & Bradley, A. M. Slow-slip evolves into megathrust earthquakes in 2D numerical simulations. *Geophys. Res. Lett.* **39**, L18308 (2012).
35. Gibbs, J., Healy, J., Raleigh, C. & Coakley, J. Seismicity in the Rangely, Colorado, area: 1962–1970. *Bull. Seismol. Soc. Am.* **63**, 1557–1570 (1973).
36. Kim, W. Y. Induced seismicity associated with fluid injection into a deep well in Youngstown, Ohio. *J. Geophys. Res. Solid Earth* **118**, 3506–3518 (2013).
37. Rivet, D. et al. Seismic velocity changes associated with aseismic deformations of a fault stimulated by fluid injection. *Geophys. Res. Lett.* **43**, 9563–9572 (2016).

Acknowledgements

We used the hypocentre catalogue unified by the Japan Meteorological Agency and waveform data recorded at MeSO-net stations. S. Sakai and Y. Asano provided us with the MeSO-net waveform data. We thank A. Hasegawa and Y. Takei for discussions. This study was supported by the Earthquake Research Institute cooperative research programme (2017-D-21) and JSPS KAKENHI (grant numbers JP15K05260, JP16H04040, JP16H06475, JP16H06473, JP17K05626 and JP17H05309).

Author contributions

J.N. performed the waveform analysis, and N.U. estimated the slip rates of the megathrust using small repeating earthquakes. Both J.N. and N.U. designed this study and contributed to the interpretation of the data and preparation of the manuscript.

Competing interests

The authors declare no competing interests.

Additional information

Supplementary information is available for this paper at <https://doi.org/10.1038/s41561-018-0090-z>.

Reprints and permissions information is available at www.nature.com/reprints.

Correspondence and requests for materials should be addressed to J.N.

Publisher's note: Springer Nature remains neutral with regard to jurisdictional claims in published maps and institutional affiliations.

Methods

Slip rate estimates on the megathrust. Earthquakes that repeat on a fault are considered to occur to catch up with slip in surrounding areas, and can thus be used to estimate slip rates along the fault³⁸. We first identified repeating earthquakes from waveform similarities using the method of ref. ³⁹ for earthquakes occurring along the upper surface of the Philippine Sea slab between January 2004 and June 2015. We set the waveform coherence threshold to 0.95 for averaged coherences at 1–8 Hz, or to 0.8 for a frequency band between half and double the corner frequency of the smaller event in an earthquake pair. We estimated slip for each earthquake using the empirical relationship between the seismic moment M_0 (in dyne cm) and fault slip d (in cm), which is³⁸ $\log(d) = -2.36 + 0.017 \log(M_0)$. We calculated the seismic moment using M_{JMA} with the relationship: $\log(M_0) = 1.5M_{JMA} + 16.1$. We set three time-window lengths (0.2, 0.3 and 0.4 years) with a 0.1-year moving window, and calculated cumulative slip rates in each time window from the repeater sequences shown by the red stars in Fig. 1c. We then estimated average slip rates on the megathrust in each time window by dividing cumulative slip by the window length. We plotted the estimated average slip rates at the centre of each time window.

Correlation analysis. We carried out parametric and non-parametric analyses to calculate cross-correlation coefficients between the time series of the number of supraslab earthquakes and the average slip rates on the megathrust. For parametric analysis, we calculated the Pearson correlation coefficient, which is frequently used in correlation analysis, whereas for non-parametric analysis we calculated the Spearman rank correlation coefficient. The Pearson correlation requires that the two variables are normally distributed and homoscedastic; however, the Spearman rank correlation does not require any assumptions on data distribution⁴⁰. The Spearman rank correlation coefficient, unlike the Pearson correlation coefficient, can deal with skewed data or outliers. For the correlation coefficients from the two analyses, we calculated Student's t probability (P value) to verify the null hypothesis that supraslab earthquakes occur randomly irrespective of the megathrust slip rates.

In our correlation analysis, we calculated the number of supraslab earthquakes and average megathrust slip rates for three time-window lengths (0.2, 0.3 and 0.4 years) with a 0.1-year moving window, which discretized the time series of both processes at every 0.1 year. To remove the effect of the 2011 Tohoku-oki earthquake on seismic activity, we considered three periods (2004–2010, 2012–2015.5 and 2013–2015.5) for cross-correlation estimates. As a result, we did not obtain a statistically significant correlation between the number of supraslab earthquakes and average megathrust slip rates for 2012–2015.5 (Supplementary Fig. 2a and b). We infer that the high activity level of supraslab earthquakes caused by the static stress change of the 2011 Tohoku-oki earthquake continued until late 2012 (Fig. 2a). Therefore, we show results of correlation analyses for the two periods (2004–2010 and 2013–2015.5) in the main text.

The Pearson analysis for 2013–2015.5 yielded negative cross-correlation coefficients with small P -values (<0.01) at positive (0.5–0.7 years) and negative (0.3–0.7 years) lags (Supplementary Fig. 2b), but the Spearman analysis, which provides more robust and stable estimates, did not show such large lag times, with P -values of <0.01 (Supplementary Fig. 2a). We consider that the positive cross-correlation coefficients ($P < 0.01$) at relatively short lag times (0.2–0.4 years for 2004–2010 and 0.1 year for 2013–2015.5), which were observed independently of analysis methods and time-window lengths (Supplementary Fig. 2a and b), are robust and reliable. The cross-correlation coefficients calculated by both analyses yielded nearly identical results; therefore, we show the cross-correlation coefficients calculated using Spearman rank analysis, as it can provide a more robust and stable estimate than Pearson analysis. We hereafter show cross-correlation coefficients obtained with a 0.4-year time window length and discuss the temporal correlation between the number of supraslab earthquake and megathrust slip rates.

We observed relatively high cross-correlation coefficients at lags of 0.2 year ($CC = 0.39$ and $P = 9 \times 10^{-4}$), 0.3 year ($CC = 0.46$ and $P = 9 \times 10^{-5}$), and 0.4 year ($CC = 0.41$ and $P = 5 \times 10^{-4}$) for 2004–2010, and at a 0.1-year lag ($CC = 0.53$ and $P = 6 \times 10^{-3}$) for 2013–2015.5 (Fig. 2c). Therefore, we conclude that for 2004–2010 and 2013–2015.5, there is a moderate correlation between the number of supraslab earthquakes and megathrust slip rates at short lag times within a $<1\%$ confidence level.

To investigate whether the correlation between supraslab seismicity and megathrust slip rates is reliable, we carried out two additional analyses for 2004–2010. First, we made a scatter plot between the number of supraslab earthquakes and megathrust slip rates (Supplementary Fig. 2c). The scatter plot shows a weak positive correlation between the two variables at a 0.3-year lag; however, it does not show a positive correlation at a zero lag. This suggests that the 0.3-year lag can result in a higher correlation between the two variables.

Second, we simulated the distribution of maximum cross-correlation coefficients, assuming random occurrences of supraslab earthquakes. We produced a random time sequence of 53 supraslab earthquakes for 2014–2010 and calculated maximum cross-correlation coefficients using the same scheme we used in the actual data analysis and repeated this calculation 10,000 times. The simulated number of supraslab earthquakes ($n = 53$) corresponds to the actual number of supraslab earthquakes in 2004–2010. The maximum cross-correlation coefficients for the 10,000 trials show a normal distribution with an average of 0.28 and σ of

0.10 (Supplementary Fig. 2d). The maximum real-data cross-correlation coefficient (0.46) at a 0.3-year lag is not beyond a 2σ level, and from only this statistical test we cannot rule out the possibility that the observed temporal correlation is spurious.

The two additional analyses do not completely verify that the observed correlation in 2004–2010 is not spurious. However, given that significant correlations ($P < 0.01$) between the number of supraslab earthquakes and megathrust slip rates are commonly observed at short positive lags for both 2004–2010 and 2013–2015.5, and that seismic attenuation above the megathrust increases concurrently with megathrust slip for 2013–2015.5 ($CC = 0.78$ and $P = 7 \times 10^{-6}$ at a zero lag and $CC = 0.71$ and $P = 7 \times 10^{-5}$ at a lag of 0.1 year) (Fig. 3c), the three independent seismic parameters (megathrust slip rates, supraslab seismicity and seismic attenuation above the megathrust) are highly likely to all correlate at short positive lags. We therefore postulate that the observed correlation among megathrust slip, supraslab seismicity and seismic attenuation changes is not spurious, but rather reflects an actual physical process that occurs during and after megathrust slip.

Finally, we checked whether there is any correlation between intraslab (not supraslab) seismicity and megathrust slip rates for 2004–2010. We selected intraslab earthquakes ($M \geq 1$) that occurred in a dashed rectangle in Fig. 1a and in a distance range of 5–15 km from the upper surface of the Philippine Sea slab, and calculated the cross-correlation coefficient between the number of intraslab earthquakes and megathrust slip rates. The cross-correlation coefficients obtained do not usually show a significant correlation for three time-window lengths (0.2, 0.3 and 0.4 years) (Supplementary Fig. 2e). This result indicates that intraslab earthquakes, unlike supraslab earthquakes, occur independently of megathrust slip rates. This suggests that a physical process occurring in response to slow slip would have positive effects on supraslab seismicity but not on intraslab seismicity.

Estimates of corner frequency. Following the approach outlined by ref. ⁴¹, we can express a displacement amplitude spectrum for event i observed at station m as

$$A_{im}(f) = F_i \frac{1}{1 + \left(\frac{f}{f_{ci}}\right)^2} R_m(f) \exp(-\pi f^{1-\alpha} t_{im}^*) \quad (1)$$

where f is the frequency, $R_m(f)$ is the site-amplification factor, t_{im}^* is an attenuation term along a ray path between event i and station m , f_{ci} represents the source corner frequency of event i , α is a frequency-dependent term, and F_i is a combination of frequency-independent terms affected by the radiation pattern and seismic moment. By taking the spectral amplitude ratio at station m for events i and j , we obtain

$$\frac{A_{im}(f)}{A_{jm}(f)} = \frac{F_i}{F_j} \frac{1 + \left(\frac{f}{f_{cj}}\right)^2}{1 + \left(\frac{f}{f_{ci}}\right)^2} \exp[-\pi f^{1-\alpha} (t_{im}^* - t_{jm}^*)] \quad (2)$$

When we calculate the spectral ratio for co-located earthquakes, ray paths from the two earthquakes largely overlap, meaning that the attenuation term can be negligible. Thus, equation (2) can be written as

$$\frac{A_{im}(f)}{A_{jm}(f)} = \frac{F_i}{F_j} \frac{1 + \left(\frac{f}{f_{cj}}\right)^2}{1 + \left(\frac{f}{f_{ci}}\right)^2} \quad (3)$$

The calculated spectral ratio has two corners together with flat levels at the low- and high-frequency limits. When event i has a larger magnitude than event j , the lower- and higher-frequency corners correspond to the f_c values of events i and j , respectively. We can determine the optimum corner frequency values of the two earthquakes, f_{ci} and f_{cj} , and the ratio of spectral levels by fitting the theoretical source model.

We carried out a separate analysis for supraslab and megathrust seismic clusters, allowing us to use a pair of co-located earthquakes, which is required in order for us to cancel the attenuation term. We calculated spectrum amplitudes from the vertical component using a window length of 2.0 s from manually picked P-wave onset for permanent seismograph stations (white squares in Fig. 1a). We included only frequencies with a signal-to-noise ratio (S/N) ≥ 3 in the analysis. For each seismic cluster, we took an earthquake pair with a ≥ 0.5 magnitude difference and a ≤ 10 km distance between earthquakes, and calculated a P-wave spectral ratio for the earthquake pairs. When spectral ratios for a given earthquake pair were observed at five or more common stations, we fitted the ω^2 source model⁴² to the averaged spectral ratio, and then estimated f_c values for the earthquake pair using a grid-search technique in the frequency range of 1–32 Hz by minimising misfits between observed and theoretical spectral ratios (see Nakajima et al.⁴³ for further details). Supplementary Fig. 6 shows estimated f_c values for 12 supraslab and 629 megathrust earthquakes. We used these f_c values in the differential

attenuation estimate described below. We obtained a stress drop of 0.1 MPa to 10 MPa (average = 2.6 MPa) for the supraslab cluster and of 1 MPa to 100 MPa (average = 20 MPa) for the megathrust cluster.

Differential attenuation between two earthquakes. Once f_c is estimated, we can rewrite equation (2) in the following form:

$$\frac{A_{im}(f)}{A_{jm}(f)} \frac{1 + \left(\frac{f}{f_{ci}}\right)^2}{1 + \left(\frac{f}{f_{cj}}\right)^2} = \frac{F_i}{F_j} \exp[-\pi f^{1-\alpha} \Delta t_{ijm}^*] \quad (4)$$

where Δt_{ijm}^* is the differential attenuation term, which represents differential attenuation along two ray paths and is defined as $\Delta t_{ijm}^* = t_{im}^* - t_{jm}^*$. The left-hand term in equation (4) can be evaluated from observations at each frequency, and unknown parameters are included in the right-hand term. Equation (4) can be linearized by taking the logarithm of both sides:

$$\log O_{ijm}(f) = \log(F_i/F_j) - \pi \Delta t_{ijm}^* \log(e) f^{1-\alpha} \quad (5)$$

where

$$O_{ijm}(f) = \frac{A_{im}(f)}{A_{jm}(f)} \frac{1 + \left(\frac{f}{f_{ci}}\right)^2}{1 + \left(\frac{f}{f_{cj}}\right)^2}$$

When two ray paths have the same seismic attenuation (that is, $\Delta t_{ijm}^* = 0$), the right-hand term of equation (5) becomes constant over a given frequency range. For real data, the left-hand term of equation (5) may be inclined because of differential attenuation; hence, we can estimate the differential attenuation along the two ray paths using the slope of spectral ratios. Because we focus only on the slope of spectral ratio here, we shift each spectral ratio's level so that the logarithm of the average spectral ratio becomes zero over the analysed frequency range.

To estimate seismic attenuation between the supraslab and megathrust seismic clusters, we selected 60 earthquakes ($M \leq 2.5$) that occurred in the megathrust cluster beneath the supraslab cluster and used them as deeper earthquakes, event i , in equation (4). For event j , we used five supraslab earthquakes ($M \leq 2.0$). Ideally, the ray paths between event i and station m and between event j and station m should overlap above event j , which requires the use of seismograph stations directly above the earthquake pairs. In our analysis, we used seismograph stations installed as part of MeSO-net²¹. The accelerometers were installed in ~20-m-deep boreholes, and waveform data were digitized at a 200-Hz sampling frequency. The stations were installed between 2007 and 2011, and there are now around 300 MeSO-net stations. Because the eight stations used in this study (black squares in Fig. 1b) were installed before early 2009, we used waveform data from July 2009 to June 2015 in our seismic attenuation estimates.

We calculated the spectral amplitude for each waveform from the vertical component with a window length of 2.0 s from manually picked P-wave onset. In addition, we calculated a noise spectrum with a window length of 2.0 s before P-wave onset. We selected a frequency range of 15–45 Hz for computing Δt because it ensured high S/N ratios (Supplementary Fig. 3). We did not use data for a certain frequency if its S/N ratio was less than 10. Supplementary Fig. 4 shows the hypocentres of the 65 earthquakes with coloured circles and the ray paths to the eight stations as red lines for supraslab earthquakes and blue lines for megathrust earthquakes.

Supplementary Fig. 5 shows estimates of Δt^* with $\alpha = 0$. We stacked the spectral ratio calculated at the eight stations for each 0.4-year window length with a moving window of 0.1 year and fitted the average spectral ratio by

equation (5) using the least-squares method. The slopes of spectral ratios clearly vary over time, and the regression line fits data points well for each period (Supplementary Fig. 5). Because we used the same sets of five supraslab earthquakes as event j for all time epochs, we consider that temporal variation in Δt^* is not an artefact caused by selecting event j , but is instead a real feature associated with seismic attenuation changes between the supraslab and megathrust seismic clusters.

We calculated Q_p^{-1} between the earthquake pairs as $Q_p^{-1} = \frac{\Delta t_{ijm}^*}{\Delta \tau_{ijm}}$, where $\Delta \tau_{ijm} = \tau_{im} - \tau_{jm}$, and τ_{im} and τ_{jm} are the travel times from event i to station m and from event j to station m , respectively. We calculated travel times using a one-dimensional velocity model (JMA2001)¹⁸ for each earthquake. Supplementary Fig. 7 shows temporal variations in Δt^* , travel-time difference $\Delta \tau$, and Q_p^{-1} in each 0.4-year window. The average value of frequency-independent Q_p^{-1} estimated over the analysed period (July 2009 to June 2015) was $4.48 \pm 0.26 \times 10^{-3}$ ($Q_p = 210$ –236).

We evaluated the effects of frequency-dependent attenuation and uncertainties in f_c on temporal changes in Q_p^{-1} . We found that absolute Q_p^{-1} values changed when considering frequency-dependent attenuation with $\alpha = 0.27$, but that the temporal pattern was not affected (Supplementary Fig. 8). We also estimated temporal variations in Q_p^{-1} using f_c values calculated for a constant stress drop ($\Delta \sigma$). We calculated a source radius, r , using the formula of Eshelby⁴⁴, $r = \sqrt{3} \frac{7 M_0}{16 \Delta \sigma}$, and calculated f_c using the circular crack model⁴⁵, $f_c = \frac{Cv}{2\pi r}$, with C of 1.5 and v of 7.5 km s⁻¹. Using the same set of earthquake pairs in the actual analysis, we calculated temporal variations in Q_p^{-1} with the average stress drops of 2.6 MPa for supraslab seismic cluster and 20 MPa for megathrust seismic cluster (Supplementary Fig. 6). The results show Q_p^{-1} variations correlated with megathrust slip rates (SSEs) (Supplementary Fig. 9), suggesting that temporal variations in Q_p^{-1} are robust with respect to possible f_c estimate uncertainties.

Code availability. Computer code that supports the findings of this study is available from the corresponding author upon request.

Data availability. The data and observation results that support the findings of this study are available from the corresponding author upon request.

References

- Nadeau, R. M. & Johnson, L. R. Seismological studies at Parkfield VI: moment release rates and estimates of source parameters for small repeating earthquakes. *Bull. Seismol. Soc. Am.* **88**, 790–814 (1998).
- Uchida, N. & Matsuzawa, T. Pre- and postseismic slow slip surrounding the 2011 Tohoku-oki earthquake rupture. *Earth Planet. Sci. Lett.* **374**, 81–91 (2013).
- Press, W. H. et al. *Numerical Recipes in Fortran 77. The Art of Scientific Computing* (Cambridge Univ. Press, New York, NY, 1992).
- Scherbaum, F. Combined inversion for the three-dimensional Q structure and source parameters using microearthquake spectra. *J. Geophys. Res.* **95**, 12423 (1990).
- Brune, J. N. Tectonic stress and the spectra of seismic shear waves from earthquakes. *J. Geophys. Res.* **75**, 4997 (1970).
- Nakajima, J. et al. Seismic attenuation beneath northeastern Japan: constraints on mantle dynamics and arc magmatism. *J. Geophys. Res. Solid Earth* **118**, 5838–5855 (2013).
- Eshelby, J. D. The determination of the elastic field of an ellipsoidal inclusion, and related problems. *Proc. R. Soc. Lond. Ser. A* **241**, 376–396 (1957).
- Sato, T. & Hirasawa, T. Body wave spectra from propagating shear cracks. *J. Phys. Earth* **21**, 415–431 (1973).